Journal of Zhejiang University-SCIENCE A (Applied Physics & Engineering)
ISSN 1673-565X (Print); ISSN 1862-1775 (Online)
www.jzus.zju.edu.cn; www.springerlink.com
E-mail: jzus@zju.edu.cn

Parameters of a discrete element ballasted bed model based on a response surface method*

Jie-ling XIAO[1,2], Gan-zhong LIU[†‡1,2], Jian-xing LIU[1,2], Jia-cheng DAI[1,2], Hao LIU[3], Ping WANG[1,2]

[1]*MOE Key Laboratory of High-speed Railway Engineering, Southwest Jiaotong University, Chengdu 610031, China*

[2]*School of Civil Engineering, Southwest Jiaotong University, Chengdu 610031, China*

[3]*Railway Engineering Research Institute, China Academy of Railway Sciences Group Co., Ltd., Beijing 100081, China*

[†]E-mail: kevinlau@my.swjtu.edu.cn

Received Mar. 29, 2019; Revision accepted Aug. 17, 2019; Crosschecked Aug. 27, 2019

Abstract: Discrete element simulation on ballasted beds is an important method to study the service characteristics of ballasted tracks; an effective simulation should be based on proper ballast parameters. Ballast contact parameter, which exhibits a high discreteness affected by factors such as material, shape, and gradation, can effectively be calibrated by an angle of repose test. Based on the testing principles of a multi-parameter response surface method, the Box–Behnken method is adopted to design the angle of repose test under the influence of restitution, static friction, and rolling friction coefficients; laboratory-measured results are combined with the simulation; regression analyzed angle of repose is considered as the goal; parameters optimization and ballasted bed resistance simulations are verified for multiple parameters. The results demonstrate that Chinese special-grade ballasts exhibit an average laboratory-measured angle of repose of (39.78±1.27)°, and the optimal combination of parameters in this discrete element simulation based on the response surface method are as follows: the restitution coefficient is 0.72, the static friction coefficient is 0.56, and the rolling friction coefficient is 0.27. The results of the lateral resistance simulation are in accordance with the laboratory test, indicating that the optimal parameters are usable. The multi-parameter response surface method effectively helps calibrate the parameters of the discrete element simulation on ballasted beds.

Key words: Ballasted track; Ballast; Discrete element method; Parameter; Calibration; Response surface method
https://doi.org/10.1631/jzus.A1900133 **CLC number:** U213.7

1 Introduction

Ballasted tracks have been widely utilized owing to their low construction cost, short construction cycle, convenient and fast maintenance, good vibration damping performance, strong drainage capacity, and cost effectiveness (Esveld, 2001). However, ballasted tracks comprise several loose gravel particles, and therefore, the track structure exhibits high discreteness (Xiao et al., 2017). The material properties, geometry, and nesting and interlocking of the ballast particles have a considerable impact on the macroscopic force transfer behavior, micromechanical mechanism, and long-term serviceability of ballasted beds (Indraratna et al., 2011). The discrete element method can be used to study the microscopic characteristics of ballast. Cundall (1971a, 1971b) first proposed the discrete element method and used it to study the rock landslide phenomenon. The simulation results are considerably consistent with practical values and can better reflect the granular characteristics of rocks (Cundall, 1971a, 1971b; Cundall and Strack, 1980). Tutumluer et al. (2012), Huang and Tutumluer (2014), and Chen and Bian (2018) used

‡ Corresponding author

* Project supported by the National Funds for Distinguished Young Scientists of China (No. 51425804) and the Postdoctoral Innovative Talent Support Program of China (No. BX20190388)

ORCID: Jie-ling XIAO, https://orcid.org/0000-0002-4692-7464; Gan-zhong LIU, https://orcid.org/0000-0001-5761-7616

discrete element method to comprehensively study the shear characteristics of railway ballast, and they analyzed the influence of different direct shear pressures on the mechanical properties of ballast. Some researchers studied the reinforcement performance of the geogrid on the ballasted bed by combining discrete element method and a laboratory test (McDowell et al., 2006; Indraratna et al., 2014; Ngo et al., 2014, 2017). Some researchers studied the vibration characteristics of ballast using the discrete element method (Cheng et al., 2005; Lu and McDowell, 2006; Ngo et al., 2017). All these studies demonstrate that the discrete element method can better reflect the granular mechanical characteristics of railway ballast.

However, for such studies, it is crucial to select proper model parameters to conduct effective simulations. Discrete element simulation generally requires two types of basic particle parameters: intrinsic parameters, such as the density of a material, Poisson's ratio, Young's modulus, and shear modulus, and contact parameters, such as the coefficient of restitution, coefficient of static friction, and coefficient of rolling friction (Cundall, 1971a, 1971b; Cundall and Strack, 1980). An intrinsic parameter is an intrinsic property of the material that can be directly measured using testing samples of the material. The material uniformity of ballast is poor, particle size varies, shape difference is considerable, and ballast quality is considerably affected by the production process. Therefore, the intrinsic parameters have a certain variability, and a statistical analysis is required for the simulation tests. Contact parameters are related to material properties, particle surface characteristics, contact morphology, aggregate state, and geometric properties. The coefficient of restitution helps determine the ability of the particles to recover after collisions, the coefficient of static friction characterizes the resistance of the particles to sliding, and the coefficient of rolling friction characterizes the resistance of the particles to rolling.

Researchers have conducted many studies to analyze the parameters of ballast. Indraratna and Salim (2005), Diyaljee (2013), and Biabani et al. (2016) comprehensively investigated the interactions and mechanical properties of ballast particles in different application stages through a series of laboratory experiments including triaxial compression and direct shear tests. Huang et al. (2009) and Qian et al. (2015) studied the micro-mechanical parameters of ballast using triaxial compression tests. Xu et al. (2016) determined the coefficient of friction of the ballast to be approximately 0.6 via an angle of repose test. Aursudkij et al. (2009) tested the volume change, elastic modulus, Poisson's ratio, and other parameters of ballast under various axial strains through large-scale triaxial tests. Based on the above studies, certain parameters in discrete element models were adopted from physical parameters obtained through specific tests, such as the triaxial, direct shear, and angle of repose tests. However, ballasted beds are characterized by considerable variations in particle size and other characteristics, and their macroscopic mechanical properties are determined based on multiple factors. A single test repeated a limited number of times cannot satisfy the requirement to study multiple parameters. A response surface method is a statistical method that can realize experimental design under various conditions; therefore, it may be a feasible approach to solve the problem of ballast parameter selection. The response surface method was introduced by Box and Wilson (1951). This method employs a well-designed finite-order orthogonal experiment to obtain partial data, and then identifies the set of optimal parameters by fitting multiple high-order regression equations to solve multivariate optimization problems (Box and Wilson, 1951). Chehreghani et al. (2017) employed the response surface method to study the parallel-bond tensile strength, cohesion strength, elastic modulus, friction angle, and stiffness of the discrete model of rock samples. Based on the response surface method and employing the Plackett–Burman test, Liu et al. (2016) screened the significant parameters of the discrete element model for wheat. Through an experiment designed using the Box–Behnken method, they established a quadratic regression model for the angle of repose and other significant parameters of wheat and determined the optimal parameters for a wheat discrete element (Liu et al., 2016).

In this study, we determined the macroscopic characteristics of ballast, combined this information with the discrete element microscopic analysis model, and used the response surface method to explore techniques for determining the parameters of the discrete element simulation model of the ballast without breaking.

2 Calibration method for ballast particle parameters based on response surface method

Angle of repose testing is a commonly used calibration method for ballast particle parameters (Dong et al., 2008). However, only a limited number of tests can be used to analyze a single test parameter, and not all the parameters required for establishing a discrete element model can be obtained. Iterative numerical inversion is performed to assemble various combinations of different parameter values. This method is highly random, time-consuming, laborious, and not very effective. The response surface method refers to approximating the implicit limit state equation using a polynomial function through a series of determination experiments. By properly selecting the test points and iterative strategies to ensure that the polynomial function can converge on the probability of failure of the real implicit limit state equation (Khuri and Mukhopadhyay, 2010), it can effectively overcome the problem associated with a single laboratory test.

In the simulation test for the angle of repose, based on the response surface method, group analysis was first performed on the parameters to be optimized according to the methodology of the experimental design and the ranges of selected values. These parameters included the coefficient of restitution, coefficient of static friction, and coefficient of rolling friction. Then, a response surface model was constructed from the response values of each group using the Weierstrass polynomial function. Finally, the model was optimized according to the actual target, and the optimized response surface model was used to predict and evaluate the test parameters of non-sampled points. The operation process is shown in Fig. 1.

As depicted in Fig. 1, the design of the experiment and the construction of the response model play a crucial role in the response surface method.

The common methods of experimental design for response surface methodology include central composite designs (CCDs) and Box-Behnken designs (BBDs). The BBD method can evaluate nonlinear effects of three to seven factors (Ferreira et al., 2007). Each factor always has three levels: high, middle, and low; however, all factors are not arranged simultaneously at a high level of test combinations. Taking the three-factor and three-level test condition as an example, the factor levels are coded as high and low, which correspond to the maximum and minimum limits, respectively, or the middle, which corresponds to the midpoint or the average of the high and low limits obtained by linear interpolation. As the BBD uses only the center points for condition design while excluding the axial points, its conditions are standard. This method was used to study the parameters of the ballast discrete element model.

According to the Weierstrass polynomial approximation theorem, any function can be approximated by a polynomial. Therefore, when the response surface method is used for parameter optimization, the polynomial regression can be used to construct the response surface model for the solution. As such, the solution of the actual problem in the form of the polynomial regression function can be given as

$$\hat{y} = a + \sum_{i=1}^{n} b_i x_i + \sum_{i=1}^{n} c_i x_i^2 + \cdots + \sum_{i=1}^{n} d_i x_i^n + \sum_{i,l=1}^{n} \sum_{j,m=1}^{n} e_{ij} x_i^l x_j^m, \tag{1}$$

where $\hat{y}$ is a polynomial regression function constructed by the response surface method; x_i and x_j (i, j=1, 2, …, n) are the test parameters; m and n are positive integers; a, b, c, d, and e are the undetermined coefficients. Next, we used an example of the use of special-grade ballast in Chinese high-speed railway to illustrate the application of the response surface method in the selection of discrete element model parameters for the ballasted bed.

This study, taking Chinese high-speed railway special-grade ballast as an example, illustrates the application of response surface method in the selection of discrete element model parameters of ballasted bed.

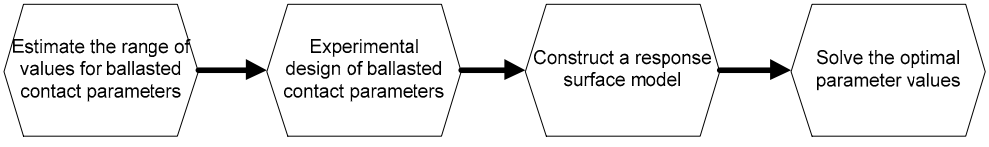

Fig. 1 Flow chart of the response surface method

3 Selection of indicator parameters and target test

3.1 Selection of indicator parameters

Ballast is commonly composed of basalt or high-grade granite; its intrinsic properties are as follows: Poisson's ratio is 0.24, density is 2600 kg/m^3, and Young's modulus is 5.45×10^{10} Pa. The ranges of contact parameters are shown in Table 1 (Liu, 2018).

Table 1 Ranges of the main contact parameters of the ballast (Liu, 2018)

Parameter	Range
Coefficient of restitution, A	0.5–1.0
Coefficient of static friction, B	0.5–1.0
Coefficient of rolling friction, C	0–0.3

Tests commonly used to calibrate ballast parameters include the direct shear test, triaxial test, and angle of repose test. Both direct shear test and triaxial test require an external force to be introduced; violent movement and fragmentation of the particles often occur during the test, making it difficult to observe and analyze the test results. The angle of repose usually refers to the relatively stable angle formed between the free surface and the horizontal plane of the granular material during natural accumulation under gravity (Komar, 1978). The angle of repose indicates the stacking capacity and state of granular materials, and it is closely related to the stability and flowability of the particles. The smaller the angle of repose, the better the flowability of the granular material, and the less likely is the stabilization of the granular material. Moreover, there is no external force introduced in the angle of repose test; thus, fragmentation of particles can be avoided in this process. The flowability of the granular material is determined by multiple parameters, including coefficient of static friction, coefficient of rolling friction, and coefficient of restitution of the particles (Matuttis et al., 2000). Therefore, the angle of repose is the macroscopic representation of the intrinsic parameters and contact parameters of each particle in the granular body (Li, 2005). The stacking capacity of a railway ballasted bed can be considered as an overall indication of the mechanical properties of the ballast stack. Evaluating these properties macroscopically with the angle of repose has become a commonly used comprehensive technical indicator for the parameter calibration used by researchers during simulation (Dong et al., 2008). Therefore, the angle of repose test was used to study the contact parameters of the ballast.

3.2 Test of angle of repose for calibration of special-grade ballast parameters

The concept of the particle angle of repose is clear; however, it is difficult to obtain accurate measurements. At present, there are three types of test methods: injection, discharge, and tilting (Dong et al., 2008). To reduce the influence of the boundary on the test and test costs, the injection method was used to study the angle of repose of the ballast.

Prior to the test, valid test samples were obtained by screening the ballast according to the grading requirements of the special-grade ballast used for high-speed railways. The sieving mass curve is shown in Fig. 2. The ballast samples had a maximum particle size of 62.5 mm.

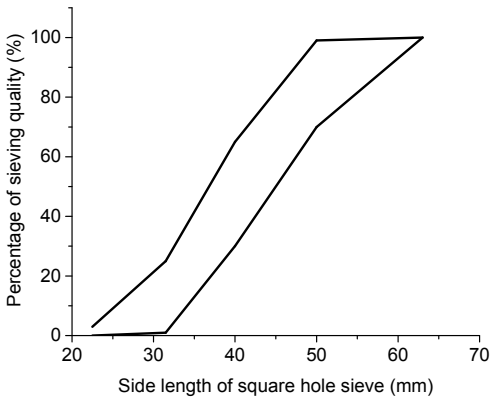

Fig. 2 Ballast grading curve

According to the theory of granular test (Wu et al., 2002), the test cylinder had a diameter of 250 mm (4–5 times the maximum particle size) and a height of 900 mm (3–4 times the diameter of the cylinder). The material used was poly vinyl chloride. The inner surface of the cylinder was extremely smooth compared with the ballast to reduce the effect of interface friction on the test. The test cylinder was erected on level ground. The measured coefficient of static friction of the ballast and the ground was 0.52. The test cylinder was filled with special-grade ballast and slowly lifted by an elevator at a speed of 10 mm/s to allow the ballast to accumulate naturally. After the

ballast slid out from the bottom of the cylinder and was stabilized, a naturally accumulated ballast stack was obtained. As shown in Fig. 3a, the stack was cone shaped.

The ballast particles scattered outside the stack were removed. All the ballast particles present in the stack were retained. The height H of the vertex from the ground and the horizontal distance L from the center of the stack to the circumference of the bottom of the stack were measured. Considering the randomness of the granular material and the measurement error, there were certain differences in the angle of repose in each direction. As such, the cone was divided into n equal parts by the vertices, and L in n directions were measured; these measurements are denoted by L_i (i=1, 2, …, n). The measurement at n=4 is shown in Fig. 3.

Rackl and Grötsch (2018), Roessler and Katterfeld (2018), and Shorts and Feitosa (2018) studied the specific angle of repose of the accumulated body through the image recognition method and proposed a nonlinear description method for the angle of repose. However, the model could not reflect the state dependence and environmental sensitivity of the ballast.

Fig. 3 Test process for angle of repose
(a) Natural accumulation process; (b) Top view of ballast pile; (c) Front view of ballast pile

To eliminate the errors in the test, the traditional linear description method was used for measurements in the laboratory test and the simulation results of the angle of repose of ballast. Each test was repeated 10 times, and the mean value of L (denoted by $\overline{L}$) was calculated using the measured H and L values recorded in the tests. The results are summarized in Table 2.

In the angle of repose test, the angle of repose varied in different directions. To obtain a representative angle, the results measured in all directions were averaged using (Guo et al., 2014)

$$\alpha = \arctan\frac{nH}{\sum_{1}^{n} L_i}. \tag{2}$$

According to Li (2005), when n≥4, the measured angle of repose can adequately represent the angle of repose of the ballast stack. For n=4, the representative value for the ballast angle of repose from each test is shown in Fig. 4.

The average of the angle of repose is denoted by $\overline{\alpha}$, standard deviation of the measurement by $\hat{\sigma}$, and standard deviation of the arithmetic mean by $\hat{\sigma}(\overline{\alpha})$. According to the theory of experimental error, these quantities can be obtained as follows:

$$\overline{\alpha} = \frac{\alpha_1 + \alpha_2 + \cdots + \alpha_{10}}{10} = 39.78°, \tag{3}$$

$$\hat{\sigma} = \sqrt{\frac{(\alpha_1 - \overline{\alpha})^2 + (\alpha_2 - \overline{\alpha})^2 + \cdots + (\alpha_{10} - \overline{\alpha})^2}{10 - 1}} = 4.02°, \tag{4}$$

$$\hat{\sigma}(\overline{\alpha}) = \frac{\hat{\sigma}}{\sqrt{10}} = 1.27°. \tag{5}$$

Therefore, the values of the angle of repose α and relative error E_r are given by

$$\alpha = \overline{\alpha} \pm \hat{\sigma}(\overline{\alpha}) = (39.78 \pm 1.27)°, \tag{6}$$

$$E_r = \frac{\hat{\sigma}(\overline{\alpha})}{\overline{\alpha}} \times 100\% = 3.19\%. \tag{7}$$

The analysis showed that the average angle of repose of the test ballast was 39.78°, the standard deviation was 4.02°, and the relative error was 3.19%. Because the relative error was less than 5%, which reflects the criterion error value allowed by the general test (Morris and Langari, 2016), the test results have a high reliability.

Table 2 Test results

Test number	H (mm)	L_1 (mm)	L_2 (mm)	L_3 (mm)	L_4 (mm)	$\overline{L}$ (mm)
1	32.6	36.0	39.5	43.0	35.6	37.34
2	32.3	36.0	25.0	31.0	36.0	32.06
3	32.0	36.0	45.0	35.0	31.5	35.90
4	31.0	35.0	27.0	36.0	29.0	31.60
5	29.5	30.0	42.0	39.5	37.0	35.60
6	27.0	40.0	39.0	40.0	52.0	39.60
7	28.7	43.0	39.0	37.0	36.0	36.74
8	29.0	35.0	37.0	43.0	30.0	34.80
9	30.0	27.0	31.0	34.0	33.0	31.00
10	27.4	31.0	42.0	41.0	29.0	34.08

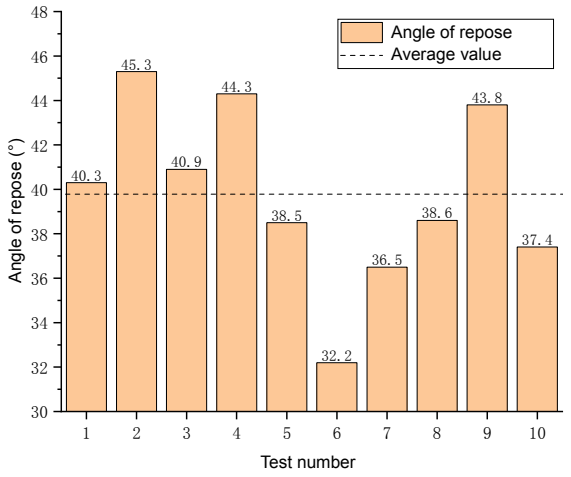

Fig. 4 Test results and residual errors of angle of repose test

4 Numerical test of discrete element parameters based on response surface method

4.1 Discrete element particle constitutive model

In the discrete element method, the physical-mechanical properties between particles are achieved by using the contact constitutive model between particles. The Hertz–Mindlin (no slip) model is a commonly used mechanical constitutive model in the discrete element method. This model is highly efficient and accurate for the calculation of the force; therefore, it has been widely used by researchers. The

discrete element model below is based on the Hertz–Mindlin (no slip) contact constitutive model.

In the Hertz–Mindlin (no slip) model, the normal force F_n is a function of the normal particle overlaps δ_n (Hertz, 1881):

$$F_n = \frac{4}{3} E^* \times \sqrt{R^*} \times \delta_n^{3/2}, \tag{8}$$

where E^* is the equivalent Young's modulus of the particles, and R^* is the equivalent radius of the particles; they are defined as

$$\frac{1}{E^*} = \frac{1-\mu_i^2}{E_i} + \frac{1-\mu_j^2}{E_j}, \tag{9}$$

$$\frac{1}{R^*} = \frac{1}{R_i} + \frac{1}{R_j}, \tag{10}$$

where E_i and E_j, μ_i and μ_j, and R_i and R_j are Young's moduli, Poisson's ratios, and the radii, respectively, of the contact sphere of the two particles.

The tangential force F_t depends on the tangential particle overlaps δ_t and the tangential stiffness S_t (Mindlin, 1949; Mindlin and Deresiewicz, 1953) as shown in the following equations:

$$F_t = -S_t \delta_t, \tag{11}$$

$$S_t = 8G^* \sqrt{R^* \delta_n}, \tag{12}$$

where G^* is the equivalent shear modulus of the particles.

In addition, the expressions of the normal damping force F_n^d and tangential damping force F_t^d (Tsuji et al., 1992) are as follows:

$$F_n^d = -2\sqrt{\frac{5}{3}} \beta \sqrt{S_n m^*} v_n^{\overline{rel}}, \tag{13}$$

$$F_t^d = -2\sqrt{\frac{5}{6}} \beta \sqrt{S_t m^*} v_t^{\overline{rel}}, \tag{14}$$

where $v_n^{\overline{rel}}$ and $v_t^{\overline{rel}}$ are the normal and tangential components of the relative velocity between the particles, respectively, m^* is the equivalent mass of the particles, β is the damping constant, and S_n is the normal stiffness of the particles. These variables are defined in the following equations:

$$m^* = \left(\frac{1}{m_i} + \frac{1}{m_j} \right)^{-1}, \tag{15}$$

$$\beta = \frac{\ln e}{\sqrt{\ln^2 e + \pi^2}}, \tag{16}$$

$$S_n = 2E^* \sqrt{R^* \delta_n}, \tag{17}$$

where m_i and m_j are the masses of any two particles, and e is the coefficient of restitution.

The relative motion between the particles is limited by the Coulomb friction force $\mu_s F_n$, where μ_s is the coefficient of static friction (Cundall and Strack, 1980).

The rolling friction in the constitutive model is not negligible. It is represented by a moment of force τ_i applied on the contact surface (Sakaguchi et al., 1993) as follows:

$$\tau_i = -\mu_r F_n R_i \omega_i, \tag{18}$$

where μ_r is the coefficient of rolling friction, R_i is the distance from the contact point to the center of mass, and ω_i is the unit angular velocity vector of the object at the point of contact.

According to the constitutive equation of the Hertz–Mindlin (no slip) contact model, the final parameters to be determined when using it to solve the discrete element are the particle radius, density, relative velocity, Young's and shear moduli, Poisson's ratio, and the coefficients of restitution, static friction, and rolling friction. The radii of the contact spheres are obtained when the discrete element model is being established. The relative velocity of the particles is determined by iteratively calculating their motion. Since ballast is composed of basalt or high-grade granite, it is generally considered an isotropic material (Wang and Yang, 2001). Out of the three parameters of the ballast particles (i.e. Young's modulus E, shear modulus G, and Poisson's ratio μ), only two need to be determined; the third parameter can be calculated using

$$G = \frac{E}{2(1+\mu)}. \tag{19}$$

In summary, when the Hertz–Mindlin (no slip) contact constitutive model is used to simulate ballast, the parameters to be determined are density, Young's modulus, Poisson's ratio, and the coefficients of restitution, static friction, and rolling friction.

4.2 Simulation model for ballast based on the discrete element method

Taking the laboratory-tested angle of repose as the objective, the particle discrete element model simulation test was used to calibrate the ballast contact parameters. To obtain particle shapes close to those of the test ballast, the 3D profiles of specific ballast samples were scanned with a 3D scanner and introduced into the discrete element simulation platform (Liu et al., 2019). A single ballast particle was constructed using the clump method and the cylinder was simulated using a wall in the discrete element method. The surface of the wall of the test cylinder was smooth in the laboratory test; therefore, the friction coefficient of the test cylinder in the discrete element simulation was set to 0. The test cylinder was filled with ballast using the "falling rain method." The ballast grading (MOR, 2008) used in the simulation is shown in Fig. 5.

The simulation test cylinder was raised at a constant speed of 10 mm/s, and the discrete element ballast particles fell freely under the action of gravity. After the drop ended and was stabilized, the angle of repose of the ballast in the discrete element simulation was measured. The process is shown in Fig. 6.

4.3 Design of ballast discrete element model simulation based on the response surface method

The contact parameters of the special-grade ballast listed in Table 1 were coded as high, middle, and low. The BBD method was used to select three center points for evaluation. There were 15 sets of test conditions in total, as shown in Table 3.

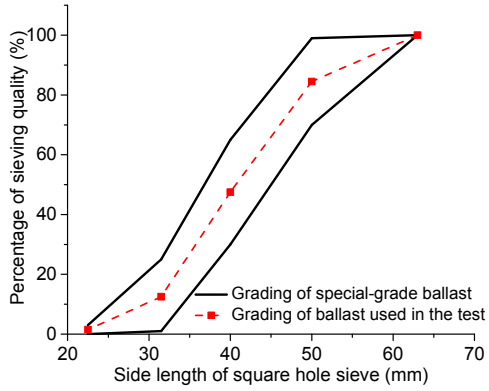

Fig. 5 Ballast grading curve used in the simulation

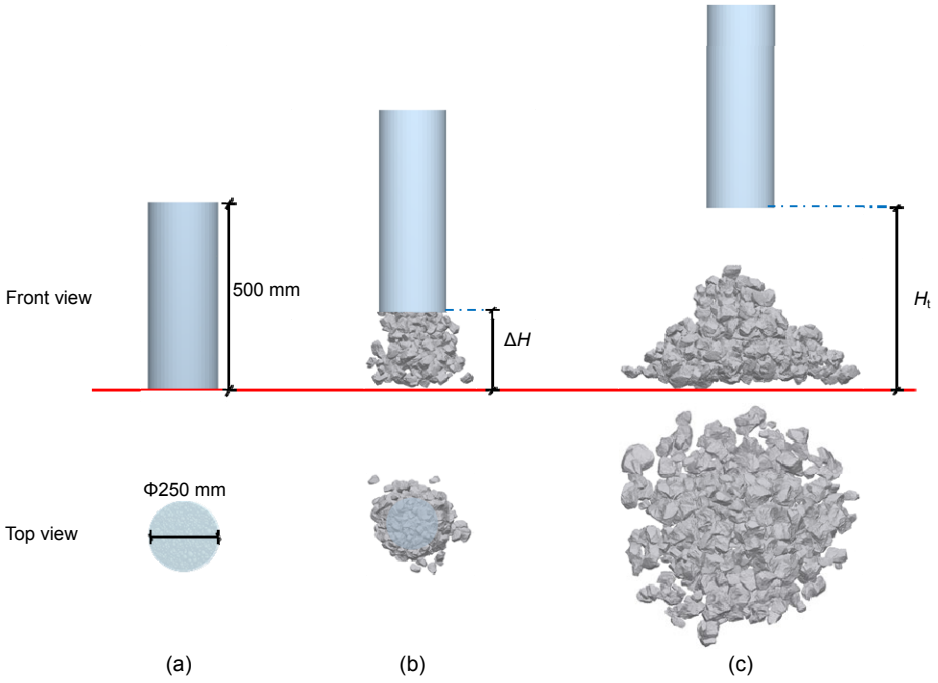

Fig. 6 Simulation process
(a) Initial moment; (b) Intermediate moment; (c) Last moment

Table 3 BBD experiment for contact parameters for special-grade ballast

Test number	*A*	*B*	*C*
1	0.75	1.00	0.30
2	0.50	0.75	0.30
3	0.75	0.50	0.00
4	0.75	0.75	0.15
5	0.75	0.75	0.15
6	0.50	0.75	0.00
7	0.75	1.00	0.00
8	1.00	0.50	0.15
9	0.75	0.50	0.30
10	0.50	0.50	0.15
11	0.50	1.00	0.15
12	1.00	0.75	0.30
13	1.00	1.00	0.15
14	0.75	0.75	0.15
15	1.00	0.75	0.00

As shown in Table 3, the BBD method did not use all three factors as a combination of all high or low levels at the same time. Groups 4, 5, and 14 were the three evaluation tests for the three center points.

5 Analysis of discrete element simulation results

5.1 Regression analysis of simulation test results

The parameter combinations listed in Table 3 were placed sequentially into the discrete element simulation model for the ballast angle of repose test, and the angle of repose was numerically simulated. The result is shown in Fig. 7. In 15 groups of simulation models, the ballast angles of repose were between 10° and 40°. The probability of the ballast angle of repose exceeding 40° was relatively small. Thus, the ballast angle of repose is likely the result of the interactions of multiple parameters, and a single parameter will have only a limited impact on the overall ballast angle of repose.

The polynomial model was used to fit the data. The *p*-value algorithm (Chaubey, 1993) was used to calculate each item iteratively. The significant items with a *p*-value less than 0.1 were selected, and the variance and statistical analyses were performed using the least squares method. The results are shown in Tables 4 and 5. The polynomial regression equation of the special-grade ballast angle of repose is

$$\begin{aligned}\theta = {} & 27.73 - 25.63B + 216.87C + 132.29AB \\ & - 566.07BC + 53.91B^2 - 80.03A^2B \\ & - 196.04AB^2 + 352.53B^2C + 121.58A^2B^2,\end{aligned} \tag{20}$$

where θ represents the angle of repose of the special-grade ballast, and the meaning of the parameters corresponding to the letters *A*, *B*, and *C* are shown in Table 1.

According to the theory of significance test (Hochberg, 1988), the *F*-value of the model was 38.02 and the *p*-value was 0.0004. The *p*-value lower than 0.05 indicates that the fitting relationship is significant, while *p*-value higher than 0.1 indicates that the fitting relationship is non-significant. This indicates that the regression equation was very effective. The *F*-value of the lack of fit was 0.98 and the *p*-value of lack of fit was 0.5407 (>0.1), which indicated that the lack of fit was non-significant compared to the pure error and therefore not important. The equation of the model fits very well.

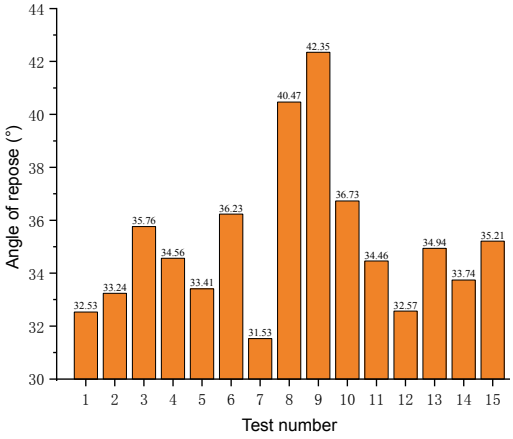

Fig. 7 BBD test results

The principle of the coefficient of determination (Bar-gera, 2017) was applied in this study. The coefficient of variation in the statistic was 1.67% (<15%), indicating that the degree of dispersion of the fitted model was relatively good. The adjusted R^2 and R^2 values were both close to 1, and the difference between them was 0.03 (<0.2), indicating that the coefficients of the model could be trusted. The fitting model had a high precision of 22.51 (>4).

Table 4 Analysis of variance

Variance source	Sum of squares	Mean square	F-value	p-value
Model	118.59	13.18	38.02	0.0004
B	49.35	49.35	142.39	<0.0001
C	7.92	7.92	22.86	0.0050
AB	2.66	2.66	7.67	0.0394
BC	7.81	7.81	22.54	0.0051
B^2	5.03	5.03	14.51	0.0125
A^2B	4.88	4.88	14.09	0.0132
AB^2	4.45	4.45	12.85	0.0158
B^2C	21.85	21.85	63.03	0.0005
A^2B^2	2.45	2.45	7.08	0.0449
Residual error	1.73	0.35	–	–
Lack of fit	1.03	0.34	0.98	0.5407
Pure error	0.70	0.35	–	–
Total	120.32	–	–	–

Table 5 Statistical analysis

Statistical parameter	Value
Standard deviation	0.59
Mean	35.18
Coefficient of variation (%)	1.67
R^2	0.99
Adjusted R^2	0.96
Precision	22.51

The two first-order terms in the fitting equation, the coefficient of static friction and the coefficient of rolling friction, were taken as an example. By assuming mean values for the other parameters, the 3D surface and the 2D curves of the relationships among the coefficient of static friction, the coefficient of rolling friction, and the angle of repose are shown in Fig. 8.

As shown in Fig. 8, there was a strong nonlinear relationship between the significant terms of the ballast discrete element parameters. When the coefficient of static friction took the middle value, the coefficient of rolling friction and the angle of repose exhibited a gradually declining linear relationship, and the coefficient of rolling friction increased as the angle of repose decreased. When the coefficient of rolling friction took the middle value, the coefficient of static friction and the angle of repose exhibited a gradually declining nonlinear relationship. The angle of repose first increased and then decreased as the coefficient of static friction increased.

5.2 Determination of optimal parameters of discrete element ballast

It can be seen from Fig. 4 that the average value of the angle of repose of the special-grade ballast in the laboratory test was (39.78±1.27)°. To determine the combinations of discrete element optimal parameters through the measured values and the response surface method, the initial design point of the optimized model was used as the starting point. The non-significant first-order item parameters were set to their respective middle values. The objective value of the selected angle of repose θ was (39.78±1.27)°. The resulting optimal parameters (two digits after the decimal point were retained) were as follows: the coefficient of restitution was 0.72, the coefficient of static friction was 0.56, and the coefficient of rolling friction was 0.27.

6 Discussion

6.1 Verification of optimal parameters of discrete element ballast

Using the above parameters, a discrete element simulation test was performed according to the method described in Section 4.2. As shown in Fig. 9, the means of the measured angles in the four sloping directions were taken as the angle of repose for each test.

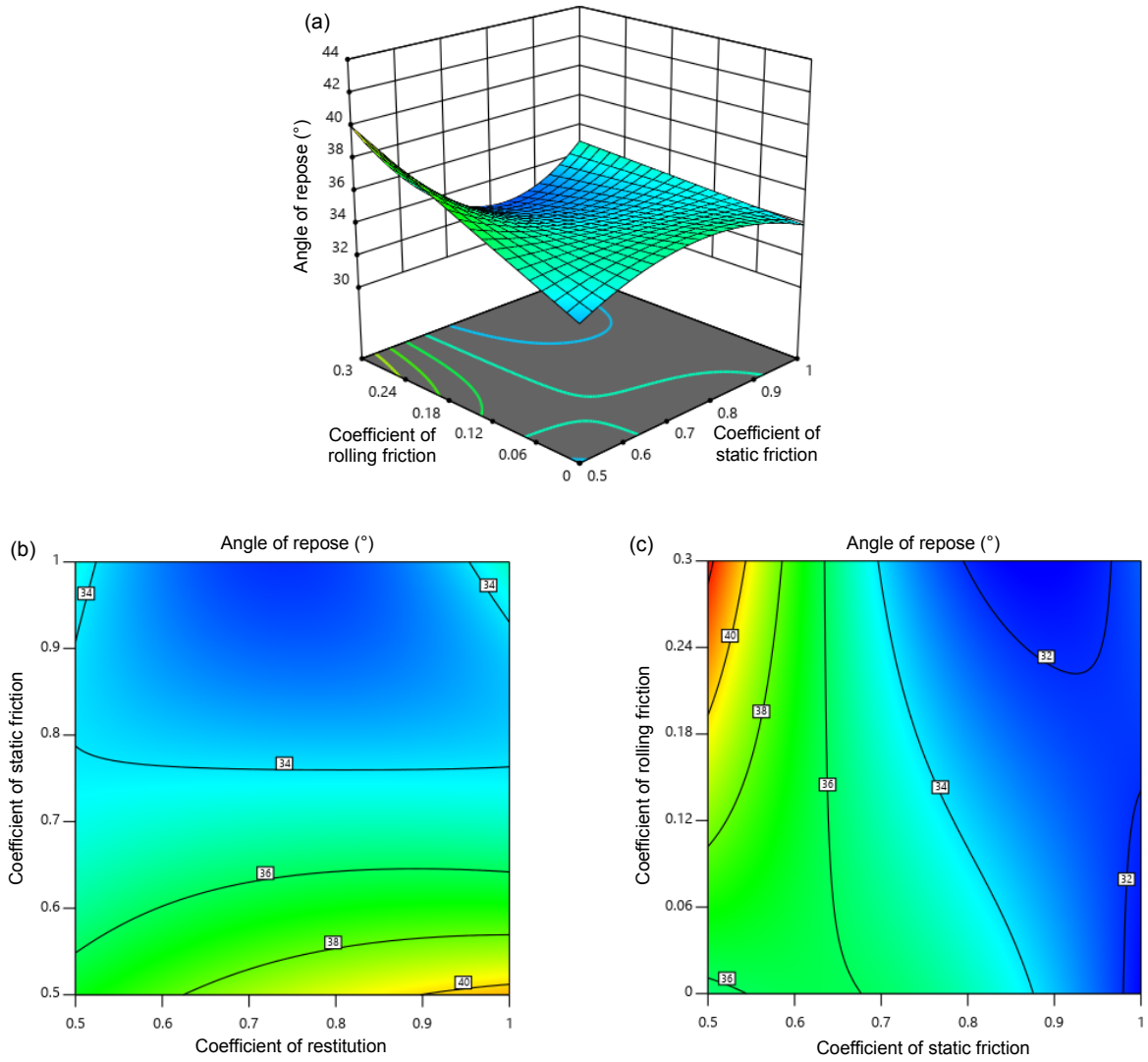

Fig. 8 Relationships among coefficient of static friction, coefficient of rolling friction, and angle of repose
(a) 3D response surface diagram of the angle of repose as a function of the coefficient of static friction and coefficient of rolling friction; (b) Contour map of the angle of repose as a function of the coefficient of restitution and coefficient of static friction; (c) Contour map of the angle of repose as a function of the coefficient of static friction and coefficient of rolling friction

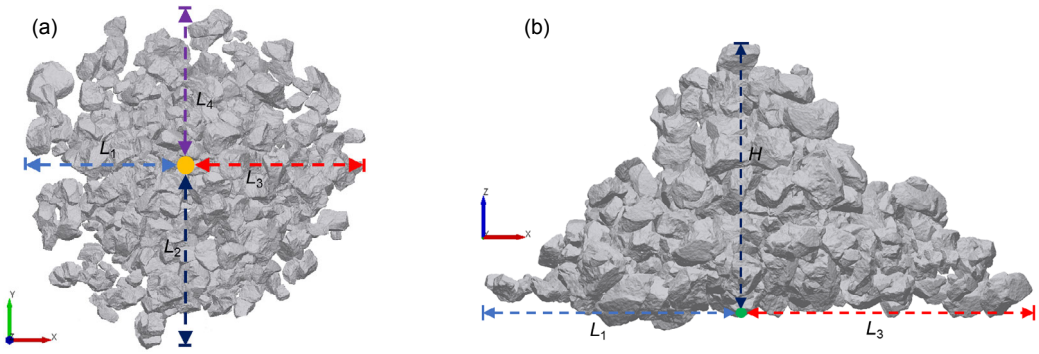

Fig. 9 Measurement of the angle of repose in discrete element ballast
(a) Top view; (b) Front view

In the three repeated tests, the angles of repose of the ballast obtained using the optimum parameters were 37.9°, 41.2°, and 39.3°. The results were subjected to a two-tailed, paired sample *t*-test, and the obtained result was p=0.65 (>0.05), indicating that the simulation test results obtained using the optimal parameters were not significantly different from the measured values (Ibragimov and Müller, 2010).

6.2 Lateral resistance test of ballasted bed based on optimal parameters of ballast

The lateral resistance of the ballasted bed is a key factor in preventing the expansion of the runway in the continuously welded rail track and ensuring track stability (Chen et al., 2017; Xiao et al., 2018). In this study, based on the discrete element method, the lateral resistance test of the ballasted bed was simulated with the obtained ballast contact parameters to verify the validity of the parameters.

According to the standard cross-sectional length of ballasted beds in China, a discrete element model of the ballasted bed consisting of three Type-III sleepers was established. Among them, the ballast was still modeled by the sphere aggregate model. The sleeper was modeled by the wall units, and gravity was applied to the wall-body sleepers through the application programming interface as shown in Fig. 10. After the model was established, the ballast volume density of the surface layer of the gravel bed model was determined to be 1.78 g/cm^3.

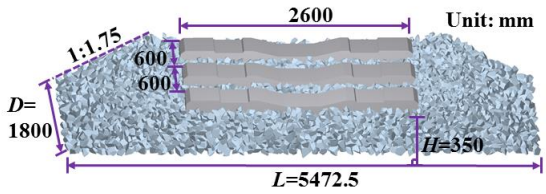

Fig. 10 Discrete element model of the ballasted bed

The lateral resistance of the ballasted bed was analyzed by pushing the middle sleeper at a constant lateral speed of 1 mm/s, as shown in Fig. 11.

As depicted in Fig. 11, once the sleeper had moved to a certain extent (i.e. a displacement of approximately 2 mm), the lateral resistance of the ballasted bed started to increase gradually with increasing lateral displacement and ultimately stabilized. The simulation results were close to the actual measurement results in the second round of testing, but they were different from the other two rounds of testing. The main reason is that, in the field test, the load was applied stepwise with jacks. Thus, the loading rate in the actual test could not be controlled as accurately as possible in the simulation. The quality of each position in the ballasted bed was different, and the quality of the simulation test of the ballasted bed was the ideal case.

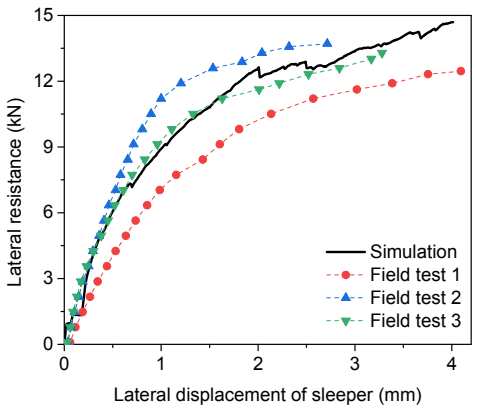

Fig. 11 Lateral resistance force of the ballasted bed

In summary, the measurements and simulation results both had certain errors that were affected by uncontrolled factors; however, the errors were small. A simulation test of the lateral resistance of the discrete element ballasted bed model agreed well with the measured results obtained in the laboratory. Thus, the process of obtaining the parameters of the discrete element model of the ballasted bed by using the response surface method worked well.

7 Conclusions and perspective

7.1 Conclusions

In this paper, the response surface method is used to study the discrete element parameters by ballast test of angle of repose. A multiple regression model was established and optimized. The contact parameters of ballast are optimized. The following results were obtained:

1. By averaging the angles of repose of the four orthogonal surfaces, the angle of repose of Chinese

special-grade ballast naturally accumulated in the laboratory was (39.78±1.27)°.

2. Taking the laboratory measured results as the objective, the simulation parameters of the special-grade ballast discrete element model were optimized using the response surface method. The variance analysis yielded two significant first-order parameters, the coefficient of static friction and the coefficient of rolling friction, as well as various combinations of a number of high-order significant parameters. The optimal model parameters were as follows: Poisson's ratio is 0.24, density is 2600 kg/m^3, Young's modulus is 5.45×10^{10} Pa, restitution coefficient is 0.72, static friction coefficient is 0.56, and rolling friction coefficient is 0.27.

3. The optimal parameters of the discrete element ballast were used to establish the discrete element model of ballasted track, and the lateral resistance test of sleeper was carried out. The simulation results were basically consistent with the laboratory tests, which indicated that the contact parameters obtained by response surface method can be used for discrete element simulation of the ballasted bed.

7.2 Perspective

Based on this paper, further research can be carried out on the following aspects:

1. In this study, the response surface method is used to statistically optimize the micro parameters of the ballast. Based on this research, the authors and their team are conducting research on the micro-mechanical parameters of ballast, hoping to explain the phenomenon of ballast accumulation from the microscopic nature.

2. In this study, the static contact parameters of ballast are calibrated through tests to determine the angle of repose of semi-static ballasts. Considering the dependence and environmental sensitivity of the ballast, the same method can be used to calibrate dynamic contact parameters of the ballast under dynamic load.

3. In view of the research status on the description method of the angle of repose, this research adopts the traditional linear description method to describe it in laboratory and simulation tests, and the final obtained contact parameter value can be verified by repeated tests. In fact, the angle of repose of the accumulated ballast is not linear. The authors and their team are studying the description mode of angle of repose, in order to describe it in a more accurate way.

4. In recent years, with the improvement of train speed and axle weight, the deterioration of ballast crushing is accelerated, the stability of the ballasted bed is insufficient, and the settlement of the ballasted bed is becoming serious, so research on ballast breaking rule and parameters needs to be conducted urgently. Based on this research, the authors and their team are conducting research on the parameters of the broken ballast, hoping to provide a way to solve the problem of deterioration of the ballasted bed.

Contributors

Jie-ling XIAO designed the research. Gan-zhong LIU processed the corresponding data and wrote the first draft of the manuscript. Jian-xing LIU and Jia-cheng DAI helped organize the manuscript. Hao LIU and Ping WANG revised and edited the final version.

Conflict of interest

Jie-ling XIAO, Gan-zhong LIU, Jian-xing LIU, Jia-cheng DAI, Hao LIU, and Ping WANG declare that they have no conflict of interest.

References

Aursudkij B, McDowell GR, Collop AC, 2009. Cyclic loading of railway ballast under triaxial conditions and in a railway test facility. *Granular Matter*, 11(6):391-401. https://doi.org/10.1007/s10035-009-0144-4

Bar-Gera H, 2017. The target parameter of adjusted *R*-squared in fixed-design experiments. *The American Statistician*, 71(2):112-119. https://doi.org/10.1080/00031305.2016.1200489

Biabani MM, Indraratna B, Ngo NT, 2016. Modelling of geocell-reinforced subballast subjected to cyclic loading. *Geotextiles and Geomembranes*, 44(4):489-503. https://doi.org/10.1016/j.geotexmem.2016.02.001

Box GEP, Wilson KB, 1951. On the experimental attainment of optimum conditions. *Journal of the Royal Statistical Society: Series B (Methodological)*, 13(1):1-38. https://doi.org/10.1111/j.2517-6161.1951.tb00067.x

Chaubey YP, 1993. Resampling-based multiple testing: examples and methods for *p*-value adjustment. *Technometrics*, 35(4):450-451. https://doi.org/10.1080/00401706.1993.10485360

Chehreghani S, Noaparast M, Rezai B, et al., 2017. Bonded-particle model calibration using response surface methodology. *Particuology*, 32:141-152. https://doi.org/10.1016/j.partic.2016.07.012

Chen HH, Bian XC, 2018. Discrete element simulation study of contact pressure distribution between sleeper and ballasts. *In*: Bian XC, Chen YM, Ye XW (Eds.), Environmental

Vibrations and Transportation Geodynamics. Springer, Singapore, p.189-195. https://doi.org/10.1007/978-981-10-4508-0_17

Chen R, Chen JY, Wang P, et al., 2017. Numerical investigation on wheel-turnout rail dynamic interaction excited by wheel diameter difference in high-speed railway. *Journal of Zhejiang University-SCIENCE A (Applied Physics & Engineering)*, 18(8):660-676. https://doi.org/10.1631/jzus.A1700134

Cheng YP, Bolton MD, Nakata Y, 2005. Grain crushing and critical states observed in DEM simulations. *In*: García-Rojo R, Herrmann HJ, McNamara S (Eds.), Powders and Grains. Taylor & Francis Group, London, UK, p.1393-1397.

Cundall PA, 1971a. A computer model for simulating progressive large scale movements in blocky rock systems. Proceedings of the Symposium of the International Society for Rock Mechanics.

Cundall PA, 1971b. The Measurement and Analysis of Accelerations in Rock Slopes. PhD Thesis, University of London, London, UK.

Cundall PA, Strack ODL, 1980. Discussion: a discrete numerical model for granular assemblies. *Géotechnique*, 30(3):331-336. https://doi.org/10.1680/geot.1980.30.3.331

Diyaljee V, 2013. Discussion of "Stress-strain degradation response of railway ballast stabilized with geosynthetics" by Buddhima Indraratna and Sanjay Nimbalkar. *Journal of Geotechnical and Geoenvironmental Engineering*, 139(12):684-700. https://doi.org/10.1061/(ASCE)GT.1943-5606.0000994

Dong YX, Song ZP, Cui SJ, 2008. Perspectives on the measurement of angle of repose. *Journal of China Pharmaceutical University*, 39(4):317-320 (in Chinese). https://doi.org/10.3321/j.issn:1000-5048.2008.04.005

Esveld C, 2001. Modern Railway Track, 2nd Edition. Delft University of Technology, Delft, The Netherlands.

Ferreira SLC, Bruns RE, Ferreira HS, et al., 2007. Box-Behnken design: an alternative for the optimization of analytical methods. *Analytica Chimica Acta*, 597(2):179-186. https://doi.org/10.1016/j.aca.2007.07.011

Guo ZG, Chen XL, Liu HF, et al., 2014. Theoretical and experimental investigation on angle of repose of biomass–coal blends. *Fuel*, 116:131-139. https://doi.org/10.1016/j.fuel.2013.07.098

Hertz H, 1881. On the contact of elastic solids. *Journal für die reine und angewandte Mathematik*, 92:156-171.

Hochberg Y, 1988. A sharper Bonferroni procedure for multiple tests of significance. *Biometrika*, 75(4):800-802. https://doi.org/10.1093/biomet/75.4.800

Huang H, Tutumluer E, 2014. Image-aided element shape generation method in discrete-element modeling for railroad ballast. *Journal of Materials in Civil Engineering*, 26(3):527-535. https://doi.org/10.1061/(ASCE)MT.1943-5533.0000839

Huang H, Tutumluer E, Dombrow W, 2009. Laboratory characterization of fouled railroad ballast behavior. *Transportation Research Record: Journal of the Transportation Research Board*, 2117(1):93-101. https://doi.org/10.3141/2117-12

Ibragimov R, Müller UK, 2010. *t*-statistic based correlation and heterogeneity robust inference. *Journal of Business & Economic Statistics*, 28(4):453-468. https://doi.org/10.1198/jbes.2009.08046

Indraratna B, Salim W, 2005. Mechanics of Ballasted Rail Tracks: a Geotechnical Perspective. Taylor & Francis, London, UK.

Indraratna B, Salim W, Rujikiatkamjorn C, 2011. Advanced Rail Geotechnology–Ballasted Track. CRC Press/Balkema, The Netherlands.

Indraratna B, Ngo NT, Rujikiatkamjorn C, et al., 2014. Behavior of fresh and fouled railway ballast subjected to direct shear testing: discrete element simulation. *International Journal of Geomechanics*, 14(1):34-44. https://doi.org/10.1061/(ASCE)GM.1943-5622.0000264

Khuri AI, Mukhopadhyay S, 2010. Response surface methodology. *Wiley Interdisciplinary Reviews: Computational Statistics*, 2(2):128-149. https://doi.org/10.1002/wics.73

Komar PD, 1978. Angle of repose. *In*: Sedimentology. Springer, Heidelberg, Germany, p.25-26. https://doi.org/10.1007/3-540-31079-7_6

Li YJ, 2005. The Experimental-simulative Study on the Granular Piling Using the Discrete Element Method. MS Thesis, China Agricultural University, Beijing, China (in Chinese).

Liu FY, Zhang J, Li B, et al., 2016. Calibration of parameters of wheat required in discrete element method simulation based on repose angle of particle heap. *Transactions of the Chinese Society of Agricultural Engineering*, 32(12):247-253 (in Chinese). https://doi.org/10.11975/j.issn.1002-6819.2016.12.035

Liu GZ, 2018. Study on Stability of Ballast Beds on Bridges Based on the Discrete Element Method. MS Thesis, Southwest Jiaotong University, Chengdu, China (in Chinese).

Liu JX, Xiao JL, Liu H, et al., 2019. Random generation method of ballast 2D topology based on particle characteristics. *Construction and Building Materials*, 221:762-771. https://doi.org/10.1016/j.conbuildmat.2019.06.131

Lu M, McDowell GR, 2006. Discrete element modelling of ballast abrasion. *Géotechnique*, 56(9):651-655. https://doi.org/10.1680/geot.2006.56.9.651

Matuttis HG, Luding S, Herrmann HJ, 2000. Discrete element simulations of dense packings and heaps made of spherical and non-spherical particles. *Powder Technology*,

109(1-3):278-292.
https://doi.org/10.1016/S0032-5910(99)00243-0

McDowell GR, Harireche O, Konietzky H, et al., 2006. Discrete element modelling of geogrid-reinforced aggregates. *Proceedings of the Institution of Civil Engineers-Geotechnical Engineering*, 159(1):35-48.
https://doi.org/10.1680/geng.2006.159.1.35

Mindlin RD, 1949. Compliance of elastic bodies in contact. *Journal of Applied Mechanics*, 16:259-268.

Mindlin RD, Deresiewicz H, 1953. Elastic spheres in contact under varying oblique forces. *Journal of Applied Mechanics*, 20:327-344.

MOR (Ministry of Railways of the People's Republic of China), 2008. Railway ballast, TB/T 2140-2008. National Standards of People's Republic of China (in Chinese).

Morris AS, Langari R, 2016. Statistical analysis of measurements subject to random errors. *In*: Morris AS, Langari R (Eds.), Measurement and Instrumentation, 2nd Edition. Academic Press, San Diego, USA, p.75-130.
https://doi.org/10.1016/B978-0-12-800884-3.00004-6

Ngo NT, Indraratna B, Rujikiatkamjorn C, 2014. DEM simulation of the behaviour of geogrid stabilised ballast fouled with coal. *Computers and Geotechnics*, 55:224-231.
https://doi.org/10.1016/j.compgeo.2013.09.008

Ngo NT, Indraratna B, Rujikiatkamjorn C, 2017. A study of the geogrid–subballast interface via experimental evaluation and discrete element modelling. *Granular Matter*, 19(3):54.
https://doi.org/10.1007/s10035-017-0743-4

Ngo NT, Indraratna B, Rujikiatkamjorn C, 2017. Simulation ballasted track behavior: numerical treatment and field application. *International Journal of Geomechanics*, 17(6):04016130.
https://doi.org/10.1061/(ASCE)GM.1943-5622.0000831

Qian Y, Mishra D, Tutumluer E, et al., 2015. Characterization of geogrid reinforced ballast behavior at different levels of degradation through triaxial shear strength test and discrete element modeling. *Geotextiles and Geomembranes*, 43(5):393-402.
https://doi.org/10.1016/j.geotexmem.2015.04.012

Rackl M, Grötsch FE, 2018. 3D scans, angles of repose and bulk densities of 108 bulk material heaps. *Scientific Data*, 5:180102.
https://doi.org/10.1038/sdata.2018.102

Roessler T, Katterfeld A, 2018. Scaling of the angle of repose test and its influence on the calibration of DEM parameters using upscaled particles. *Powder Technology*, 330:58-66.
https://doi.org/10.1016/j.powtec.2018.01.044

Sakaguchi H, Ozaki E, Igarashi T, 1993. Plugging of the flow of granular materials during the discharge from a silo. *International Journal of Modern Physics B*, 07(09n10):1949-1963.
https://doi.org/10.1142/S0217979293002705

Shorts DC, Feitosa K, 2018. Experimental measurement of the angle of repose of a pile of soft frictionless grains. *Granular Matter*, 20(1):2.
https://doi.org/10.1007/s10035-017-0774-x

Tsuji Y, Tanaka T, Ishida T, 1992. Lagrangian numerical simulation of plug flow of cohesionless particles in a horizontal pipe. *Powder Technology*, 71(3):239-250.
https://doi.org/10.1016/0032-5910(92)88030-L

Tutumluer E, Huang H, Bian XC, 2012. Geogrid-aggregate interlock mechanism investigated through aggregate imaging-based discrete element modeling approach. *International Journal of Geomechanics*, 12(4):391-398.
https://doi.org/10.1061/(ASCE)GM.1943-5622.0000113

Wang Y, Yang JH, 2001. Study on rock mass structure and mechanic property of basalt. *Chinese Journal of Rock Mechanics and Engineering*, 21(9):1307-1310 (in Chinese).
https://doi.org/10.3321/j.issn:1000-6915.2002.09.005

Wu AX, Sun YZ, Liu XP, 2002. Granular Dynamic Theory and Its Applications. Metallurgical Industry Press, Beijing, China (in Chinese).

Xiao JL, Liu H, Xu JM, et al., 2017. Longitudinal resistance performance of granular ballast beds under cyclic symmetric displacement loading. *Journal of Zhejiang University-SCIENCE A (Applied Physics & Engineering)*, 18(8):648-659.
https://doi.org/10.1631/jzus.A1700058

Xiao JL, Liu H, Wang P, et al., 2018. Evolution of longitudinal resistance performance of granular ballast track with durable dynamic reciprocated changes. *Advances in Materials Science and Engineering*, 2018:3189434.
https://doi.org/10.1155/2018/3189434

Xu Y, Gao L, Wang H, et al., 2016. Study of fractal method and influence of ballast gradation on ballast bed shear behavior. *Journal of the China Railway Society*, 38(12):94-101 (in Chinese).
https://doi.org/10.3969/j.issn.1001-8360.2016.12.014

中文概要

题　目：基于响应面法的碎石道床离散元模型参数研究

目　的：采用响应面方法研究特级道砟休止角的离散元参数仿真试验，建立多次回归模型并对其进行优化，以及对道砟接触参数进行优选。通过多参数的响应面法为碎石道床离散元参数的快速标定提供有效途径。

创新点：1. 基于响应面法对离散元道砟接触参数进行统计分析，提出道砟最优参数的回归方程及回归曲面。2. 以道砟堆积体在多个正交平面的均值为道砟休止角，构建基于一致线性描述方式的道砟休

止角实测试验与离散元仿真试验。3. 提出道砟参数的动态标定思想。

方　法： 1. 通过道砟休止角的室内试验，测量出道砟休止角度的有效均值。2. 以实测结果为目标，采用响应面法对道砟离散元仿真参数进行优选。3. 验证所提方法的可行性和有效性。

结　论： 1. 通过采用休止角的 4 个正交面取均值的方法对中国特级道砟休止角进行实测所得到的平均值为(39.78±1.27)°。2. 以实测结果为目标，采用响应面方法对特级道砟离散元仿真参数进行优选，由方差分析可得 2 个显著的一次项参数（静摩擦系数和滚动摩擦系数）以及多个显著的多次项参数组合；最优参数组合为：泊松比为 0.24，密度为 2600 kg/m^3，杨氏模量为 5.45×10^{10} Pa，碰撞恢复系数为 0.72，静摩擦系数为 0.56，滚动摩擦系数为 0.27。3. 利用特级道砟离散元最优参数建立了离散元轨排模型，并进行了轨枕横向阻力试验；仿真结果与室内试验实测阻力曲线趋势基本一致，表明响应面法获得的接触参数取值可用于碎石道床相关的离散元仿真。

关键词： 有砟轨道；道砟；离散元；参数；标定；响应面法